Electronic Supplementary Material (ESI) for Nanoscale Horizons.

Electronic Supplementary Information

Antimonene-based Flexible Photodetector

Qi Xiao,[a] Chen-Xia Hu,[a] Hao-Ran Wu,[a] Yong-Yuan Ren,[b] Xiang-Yang Li,[a] Qi-Qi Yang,[a] Guan-Hua Dun,[a] Zhi-Peng Huang,[a] Yong Peng,[c] Feng Yan,[b] Qiang Wang*[a] and Hao-Li Zhang*[a, d]

[a.] State Key Laboratory of Applied Organic Chemistry, Key Laboratory of Special Function Materials and Structure Design, College of Chemistry and Chemical Engineering, Lanzhou University, Lanzhou, 730000, P. R. China. E-mail: qiangwang@lzu.edu.cn, haoli.zhang@lzu.edu.cn.

[b.] Jiangsu Key Laboratory of Advanced Functional Polymer Design and Application, Department of Polymer Science and Engineering, College of Chemistry, Chemical Engineering and Materials Science, Soochow University, Suzhou, 215123, P. R. China.

[c.] Key Laboratory of Magnetism and Magnetic Materials of MOE, Lanzhou University, Lanzhou, 730000, P. R. China.

[d.] Tianjin Key Laboratory of Molecular Optoelectronic Sciences, Department of Chemistry, Collaborative Innovation Center of Chemical Science and Engineering, Tianjin University, Tianjin, 300072, P. R. China.

1. Additional Experimental Section

1.1 Materials

Antimony (Sb) shot was purchased from Alfa Aesar (99.9999%). N-dimethylformamide (DMF), isopropanol (IPA) and 2-butanol was purchased from Rionlon Bohua (Tianjin) Pharmaceutical& Chemical Co. Ltd. Ultrapure water was obtained with a Milli-Q System (Billerica, MA, U.S.).

1.2 Sample preparation

The synthetic routes of polymer ionic liquids (PILs) refer to the article reported by our group.[1] P([VPIm]PF_6) and P([VPIm]TFSI) were dissolved in DMF with a concentration of 16.26 mg mL^{-1} and 19.02 mg mL^{-1}, respectively. The antimony bulk was grinded in a mortar for 10 min and then they were treated within a ball-mill for 180 min at 500 rpm. The micro-crystals were then dispersed in PILs with a concentration of 1 mg mL^{-1} in ambient condition. Then the suspensions was sonicated in an ultrasonic cleaner operated at 50 kHz frequency for 3 h. A centrifugation for 3 min at 3000 rpm were carried on to precipitate the non-exfoliated bulk. A speed of 16,000 rpm was employed and the obtained precipitates were washed with DMF for three times to remove the dissolved PILs.

1.3 Characterization

The UV-Vis-NIR absorption spectra were collected on a Cary 5000 UV–vis–NIR spectrometer from Agilent. Raman spectra were obtained using a confocal microscope Raman system (Renishaw in via Raman microscope) equipped with a Renishaw CCD camera. X-ray photoelectron spectroscopy (XPS) was performed on AXIS Ultra. The height profile of the nanosheets were characterized on an Atomic Force Microscope of Agilent 5500. The TEM images were collected using a FEI Talos F200S Field Emission Transmission Electron Microscope. The SEM micrographs were obtained using field-emission scanning electron microscopy (FE-SEM, Hitachi S4800) at an accelerating voltage of 2.0 kV.

1.4 Device fabrication and measurement

The concentrated antimonene nanosheets were directly centrifugal casted on the flexible indium tin oxides/polyethylene-terephthalate ITO/PET substrate for three times to give a 5 μm thick uniform thin film, and the electrode interval was about 100 nm and the length was 0.25 cm, the width was 0.4 cm. To directly synthesize CdS quantum dots (QDs) from aqueous solution without any ligand, a sequential chemical bath deposition (SCBD)[2] method was applied. The antimonene-coated ITO substrate was successively immersed in four different beakers for about 30 seconds in each beaker. One beaker contained 0.05 M $CdCl_2$ aqueous solution, and another contained 0.05 M Na_2S aqueous solution, and the other two contained ultrapure water to remove excess precursor solution. Such a cycle was repeated for 10 times, which produces a yellow film. The CdS film which is also controlled with tapes to get the length of 0.25 cm and the width of 0.4 cm, which is just on the top of P([VPIm]PF_6) modified antimonene called Sb/P([VPIm]PF_6) film with a slip of 0.05 cm.

Photocurrent response experiments were conducted with a computer-controlled CHI660 (CHI, U.S.A.) electrochemistry workstation. I-V characteristics, flexibility test and stability test of the photodetector were measured with a Keithley 4200 SCS instrument connected to a probe station. A 500 W xenon arc lamp (at a distance of 20 cm, with a power density of 20 mW cm^{-2}) was applied as the light source.

2. Additional Characterization

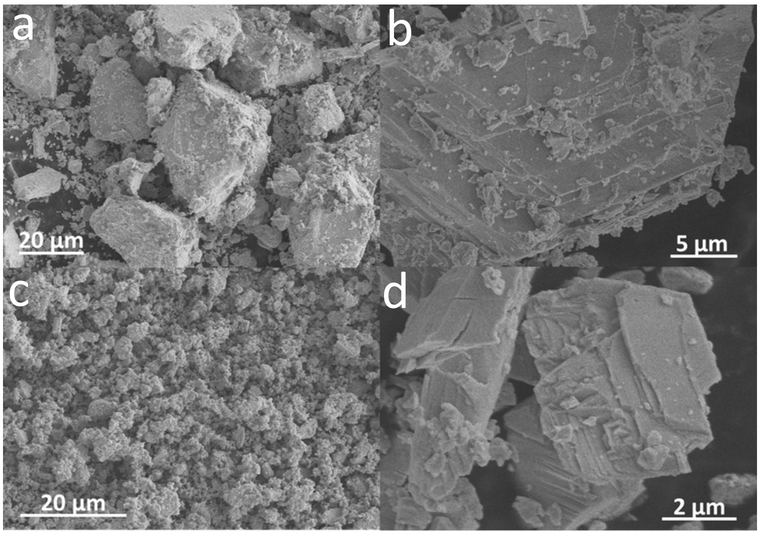

Fig. S1 SEM images of (a and b) antimony bulk after grind and (c and d) antimony micro-crystals after ball-milling.

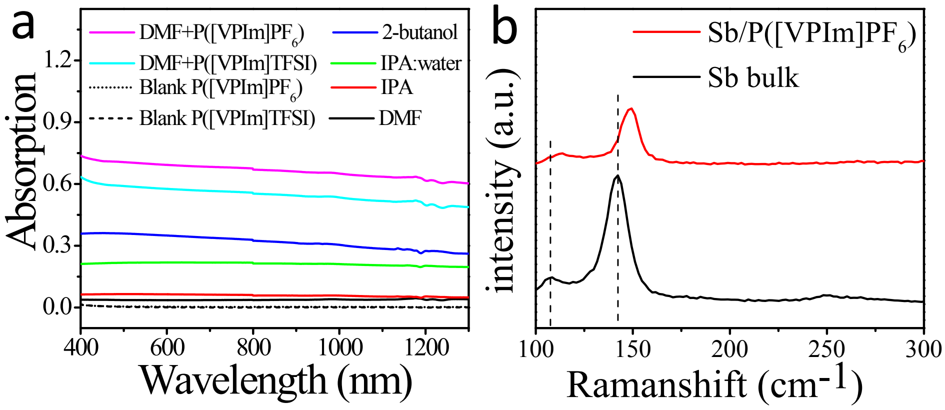

Fig. S2 (a) The absorption spectra of few layer antimonene exfoliated in DMF, IPA, IPA: water (4:1), 2-butanol, DMF+P([VPIm]TFSI), DMF+P([VPIm]PF$_6$) and the reference of pure DMF+P([VPIm]TFSI) and DMF+P([VPIm]PF_6), respectively. (b) Raman spectra of Sb/P([VPIm]PF_6) compared with antimony bulk.

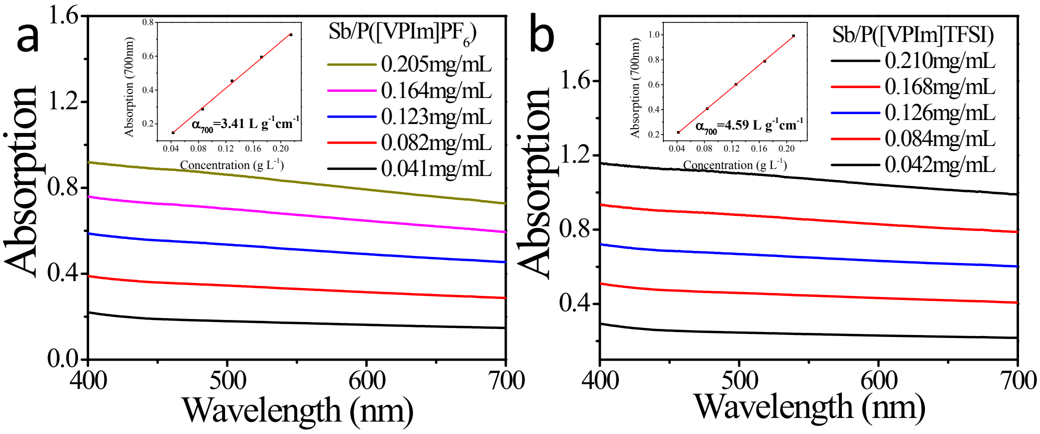

Fig. S3 The concentration-dependent absorption spectra of (a) Sb/P([VPIm]PF_6), (b) Sb/P([VPIm]TFSI), inset is normalized absorbance intensity for λ = 700 nm.

In Fig. S3, the concentration-dependent absorption spectra of Sb/P([VPIm]PF_6), Sb/P([VPIm]TFSI) was measured, inset is the test of the molecular extinction coefficient of Sb/P([VPIm]PF_6) and Sb/P([VPIm]TFSI). When the wavelength measured at 700 nm, the value are 3.41 L g^{-1} cm^{-1} and 4.59 L g^{-1} cm^{-1} for Sb/P([VPIm]PF_6) and Sb/P([VPIm]TFSI), respectively. And the each point are based on the absorption spectra. The intensity of the absorbance can reflect the concentration of the Antimonene nanosheets, the higher absorbance means higher concentration of Antimonene nanosheets in the corresponding solution. The Sb/P([VPIm]TFSI) exhibits high absorption, the corresponding concentration reaching 0.13 mg mL^{-1}. The Sb/P([VPIm]PF_6) exhibits the highest absorption in Fig. S2 among all the samples, and the concentration reaching 0.20 mg mL^{-1}, corresponding to the yield of 20%, which is, to the best of our knowledge, the highest value of liquid phase exfoliation of antimony.[3-

[6] The above results indicate that the DMF diluted PILs have an excellent ability of Antimonene exfoliation.

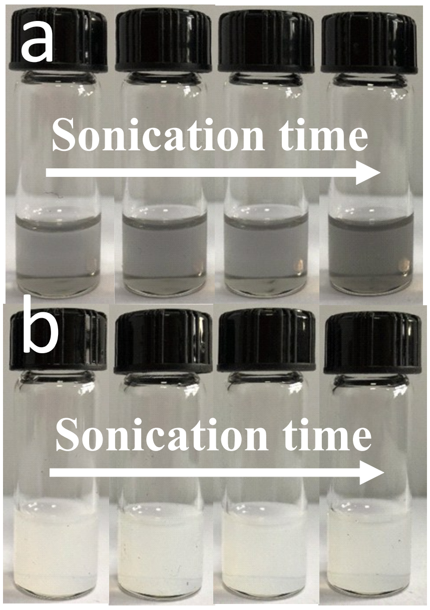

Fig. S4 Pictures of antimonene exfoliated in (a) DMF and (b) water (10 mg mL^{-1}) for 20, 40, 60 and 120 min, followed with centrifugation process at 1000 rpm for 3 min (taken after they were stood in air for 3 hours).

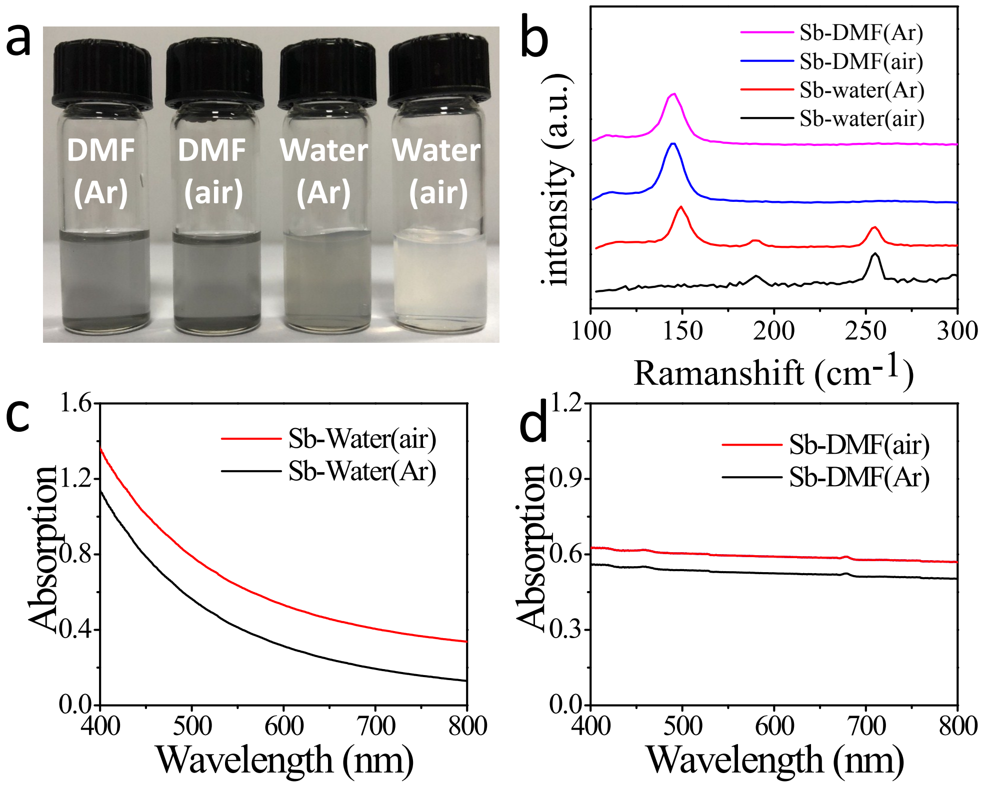

Fig. S5 (a) Pictures of antimonene exfoliated in DMF and water (10 mg mL^{-1}) at different atmosphere for 3 h, followed with centrifugation process at 1000 rpm for 3 min; (b) Raman spectra and (c and d) absorption spectra of few layer antimonene corresponding to (a).

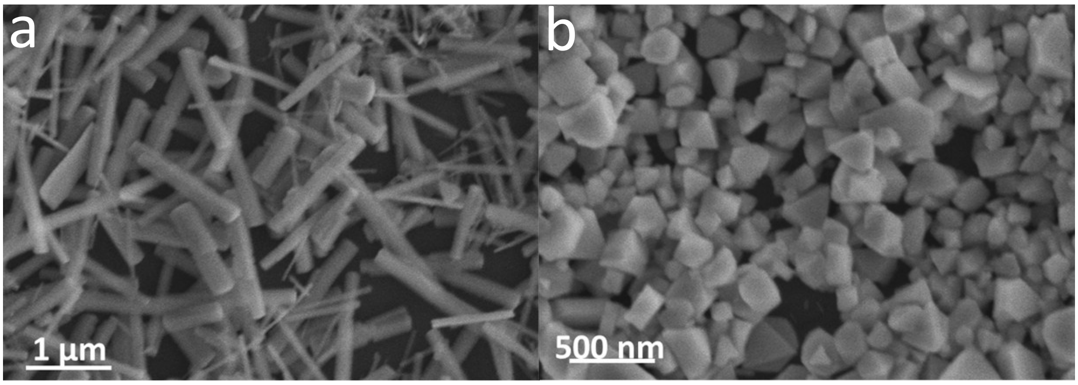

Fig. S6 SEM images of the antimony oxide result from antimony sonication in water at (a) Ar and (b) air atmosphere.

The stability of antimonene in water at different atmosphere (Fig. S5 and S6): antimony crystals were first ground in air for 5 min, and then they were placed in water (10 mg mL^{-1}) under ultrasonication for 3 h at Ar and air atmosphere. Comparative experiment was conducted in DMF with the same condition. Fig. S5a is the picture taken immediately after centrifugation process at 1000 rpm for 3 min for better comparison. When ultrasonicated in DMF, the color of the dispersions both at Ar and air are gray, match well with that in Fig. 1a. The absorption spectra in Fig. S5 also indicates the oxidation of antimonene in water whether at Ar or water atmosphere. The morphology of the products exfoliated in water was also tested, as shown in Fig. S6. The products showed rod-like and particle-like morphology at Ar and air atmosphere, respectively.

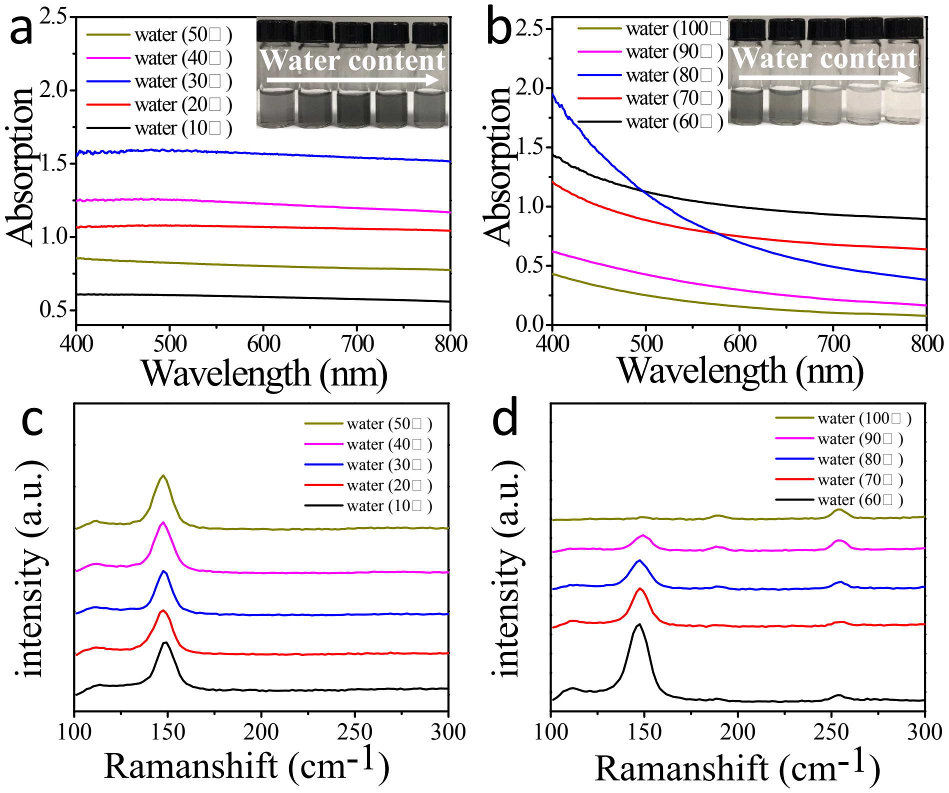

Fig. S7. Absorption spectra of few layer antimonene exfoliated under ultrasonication for 3h with water content (diluted with DMF) of (a) 10-50％ and (b) 60-100％, respectively (insets: the corresponding photographs); Raman spectra of few layer antimonene exfoliated with water content (diluted with DMF) of (c) 10-50％ and (d) 60-100％, respectively.

To further investigated the influence of different water content, the ground antimony was exfoliated under ultrasonication for 3 h with water content (diluted by DMF) of 0-100％, as shown in Fig. S7. Fig. S7a and b are the absorption spectra of antimonene colloids with water content of 10％ to 100％, and insets is the corresponding photograph of antimonene colloids. In Fig. S7a, with water content from 10％ to 50％, the absorption curves showed no obvious peak. Solution with 30％ water content showed the highest absorption and deepest color, indicating the highest exfoliating efficiency, which is due to the influence of mixed solvent. In Fig. S7b, when the water content increases from 60％ to 100％, the absorption curves show significant absorption at short wavelengths, which is consistent with Fig. 2b. And the color of antimonene colloids turn from grayish to white, indicating the oxidation states become more serious. Fig. S7c is the Raman spectra of antimonene ultrasonicated in water contents of 10％ to 50％, showing the standard two peaks of antimonene. While in Fig. S7d, with the water content increased above 60％, another two peaks appear, which correspond to antimony trioxide. As the water contents increases from 60％ to 100％, the two peaks of the antimony decreases, and the two peaks of the antimony trioxide increases continuously; Until the solution becomes pure water, Raman peaks of antimony nearly disappear, indicating that antimony became completely antimony trioxide. Above all, antimonene is stable in water, only if the water content is lower than 50％. But when the water content increased above 60％, antimonene can be gradually oxidized.

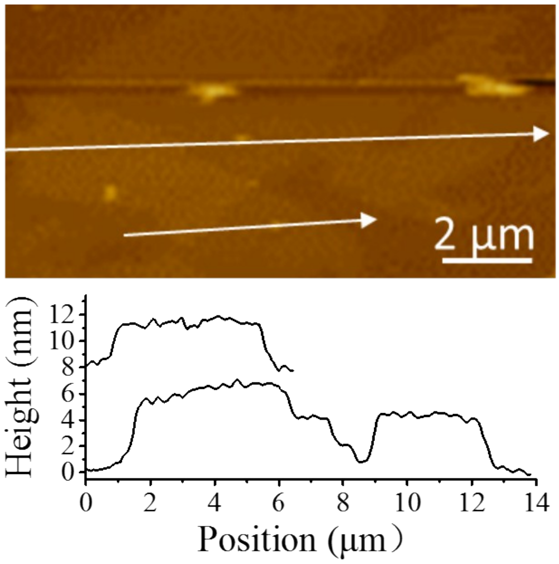

Fig. S8 AFM image of Sb/P([VPIm]PF_6) and the corresponding height profile.

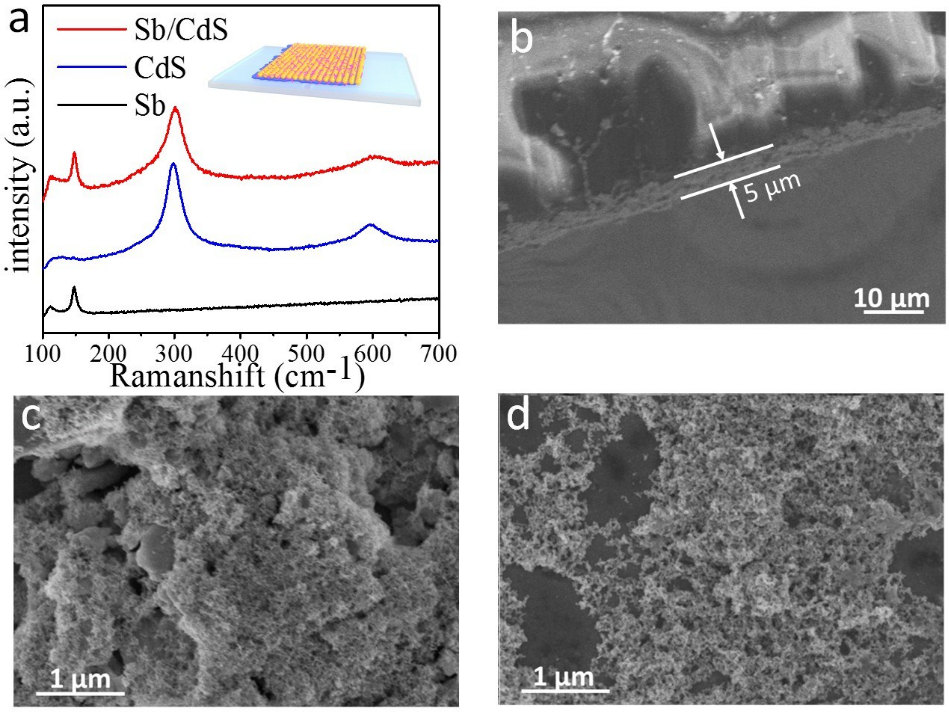

Fig. S9 (a) Raman spectra of the Sb/P([VPIm]PF_6)/CdS, CdS QDs and Sb/P([VPIm]PF_6) (inset: configuration of the Sb/P([VPIm]PF_6)-based photodetector); (b) The cross-sectional SEM images of the hybrid device; SEM images of the typical device based on (c) Sb/P([VPIm]PF_6)/CdS, and (d) CdS QDs film

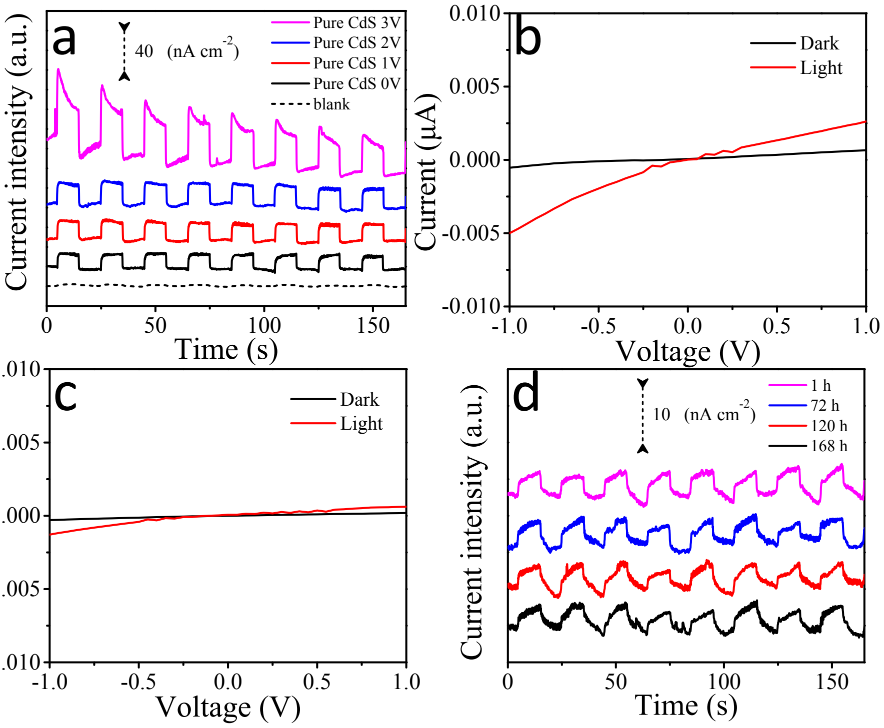

Fig. S10 Pure CdS QDs based photodetector: (a) Photocurrent density under different potential (The dashed line is the photocurrent density of reference photodetector based on pure P([VPIm]PF_6) under the bias of 3V.); (b) I-V characteristics; Sb/P([VPIm]PF_6)-based photodetector: (c) I-V characteristics; (d) Stability test.

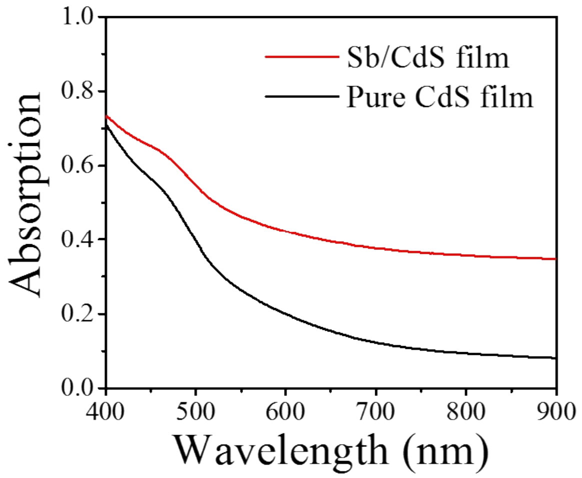

Fig. S11 Absorption spectra of CdS QDs film and the Sb/P([VPIm]PF$_6$)/CdS hybrid film

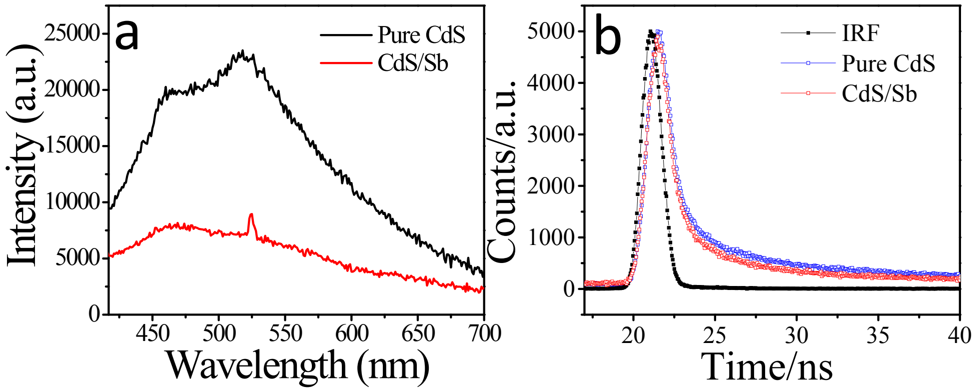

Fig. S12 (a) Photoluminescence spectra of CdS QDs and the hybrid. (b) Time-resolved fluorescence spectra of CdS QDs and the hybrid.

Table S1. Fluorescence lifetimes of samples.
(Measured at λ_{ex} = 360 nm and λ_{em} = 480 nm)

Samples	χ^2	τ_1 (ns)	τ_2 (ns)	τ_3(ns)	<τ>(ns)	B_1	B_2	B_3
CdS	1.089	0.502	4.076	23.359	1.24	0.091	0.008	0.002
CdS/Sb	0.987	0.311	2.349	12.211	0.66	0.121	0.011	0.002

$$\langle\tau\rangle = \frac{\sum_i B_i\tau_i}{\sum_i B_i}$$

Equation (1)

Fig. S12a is Photoluminescence (PL) spectra of CdS QDs and the hybrid. The fluorescence spectra of the CdS QDs shows a PL peak at 520 nm. With the hybridization of antimonene nanosheets, the emission intensity was greatly quenched, implying a possible charge transfer process between them. This result was also confirmed by Time-resolved fluorescence spectra in Fig. S12b, The decay profiles of CdS QDs and CdS/Sb were fitted with multi-exponential curves to derive three lifetime components for each. The averaged lifetimes were estimated using equation (1), where τ_i and B_i are time constants and amplitudes, respectively. The magnitudes of lifetimes and the average lifetimes $<\tau>$ are presented in Table S1. The average fluorescence lifetime was found to decrease from 1.24 ns for CdS QDs to 0.66 ns for the hybrid, further verifying the charge transfer process between them.

References

1. J. Lu, F. Yan and J. Texter, *Prog. Polym. Sci.*, 2009, **34**, 431-448.
2. C. X. Guo, H. B. Yang, Z. M. Sheng, Z. S. Lu, Q. L. Song and C. M. Li, *Angew. Chem., Int. Ed.*, 2010, **49**, 3014-3017.
3. E. Martínez-Periñán, M. P. Down, C. Gibaja, E. Lorenzo, F. Zamora and C. E. Banks, *Adv. Energy Mater.*, 2018, **8**, 1702606.
4. X. Wang, J. He, B. Zhou, Y. Zhang, J. Wu, R. Hu, L. Liu, J. Song and J. Qu, *Angew. Chem., Int. Ed.*, 2018, **57**, 8668-8673.
5. C. Gibaja, D. Rodriguez-San-Miguel, P. Ares, J. Gomez-Herrero, M. Varela, R. Gillen, J. Maultzsch, F. Hauke, A. Hirsch, G. Abellan and F. Zamora, *Angew. Chem., Int. Ed.*, 2016, **55**, 14345-14349.
6. J. Gu, Z. Du, C. Zhang, J. Ma, B. Li and S. Yang, *Adv. Energy Mater.*, 2017, **7**, 1700447.